Chapter 1

Introduction

The main theme of this thesis is the study of travelling patterns that arise as solutions of the Nagumo problem on the regular lattices $\mathbb{Z}$ and $\mathbb{Z}^2$. As the field of Lattice Differential Equations (LDEs) is relatively young compared to the classic Partial Differential Equations (PDEs) field, our knowledge of the former is pretty limited in comparison to the latter. We can divide the results for LDEs into two types.

On the one hand, we can try generalize ideas and techniques developed for PDEs, often running into technical issues. In Chapter 4 we will present some results of this type, where corner defect solutions found in the PDE setting by Haragus and Scheel [61, 60] can be constructed for LDEs as well.

On the other hand, we can think of phenomena that only occur in the spatially discrete setting but that do not find a direct translation, or at least not a well defined one, in the world of PDEs. As we will see, the results obtained in Chapters 2 and 3 regarding solutions that are asymptotically spatially periodic belong to the lattice setting and to the lattice setting only. Indeed, the structures we consider there cannot be transferred to a spatially continuous domain.

1.1 Modelling with LDEs

There are many systems in the real world where it seems more appropriate to use a spatially discrete model rather than a continuous one. Indeed, lattice equations are used in many different scientific areas [84] ranging from physics [30, 64] to dynamics of DNA strands [85, 103]. Furthermore, it is very common for numerical simulations to replace continuous variables by their discretized approximations.

Let us imagine a chain of elements in which every particle u_j is influenced by the behaviour of the two adjacent ones, u_{j-1} and u_{j+1}. We can think of modelling such behaviour with a system of the form

$$\dot{u}_j(t) = G(u_{j-1}(t), u_j(t), u_{j+1}(t)). \tag{1.1.1}$$

This is the general form of a LDE with nearest-neighbour interactions. It consists of a countable number of Ordinary Differential Equations (ODEs) that all depend on the two adjacent elements. However, we can also think of longer or even infinite range interactions [113, 124].

We are interested in solutions that take the form of a fixed shape that moves in time with some constant speed c, that is, a solution of the form $u_j(t) = \varphi(j - ct)$. We immediately see that φ would need to satisfy a particular equation, namely

$$-c\varphi'(\xi) = G(\varphi(\xi - 1), \varphi(\xi), \varphi(\xi + 1)). \tag{1.1.2}$$

Such problems are called Mixed-type Functional Differential Equations (MFDEs), due to the presence of advanced and delayed terms. Unfortunately, these problems are in general not well posed. Indeed, equation (1.1.2) needs an initial condition in the infinite dimensional space $C^0([-1, 1], \mathbb{R})$, which is not necessarily compatible with the equation itself.

Although the study of MFDEs is a fairly recent endeavour, a reasonably solid basic framework has been developed. See for example [109, 110, 93, 62] for general theory and [21, 91, 139, 140] for more focused results on travelling solutions.

FPUT equation The Fermi-Pasta-Ulam-Tsingou problem, first introduced and studied by Enrico Fermi, John Pasta, Stan Ulam and Mary Tsingou [49, 34], was designed to model a nonlinear wave in a discrete spatial setting where single atoms are chained one next to the other. This was the first attempt to model and numerically study a crystal in a one-dimensional setting. The springs between two consecutive atoms are assumed to follow Hooke's law, thus creating a linear interaction with the neighbours. Furthermore, nonlinear correction terms are taken into account, typically of quadratic (FPUT-α)

$$\ddot{u}_j = (u_{j+1} - 2u_j + u_{j-1}) + \alpha \left((u_{j+1} - u_j)^2 - (u_j - u_{j-1})^2 \right), \tag{1.1.3}$$

or cubic (FPUT-β) type

$$\ddot{u}_j = (u_{j+1} - 2u_j + u_{j-1}) + \beta \left((u_{j+1} - u_j)^3 - (u_j - u_{j-1})^3 \right). \tag{1.1.4}$$

While the authors conjectured that an initial localized impulse would eventually spread uniformly through the whole system, they later numerically found that the initial configuration was a recurring state of the system. This discovery came as a surprise, since the common idea at the time was that nonlinearity is a sufficient condition for energy diffusion. Years later, Zabusky and Kruskal [138] further numerically investigated the FPUT equation, finding a close relation to the Korteweg-de Vries (KdV) PDE

$$u_t + 6uu_x + u_{xxx} = 0, \tag{1.1.5}$$

a problem known to admit explicit soliton solutions. It took more than thirty additional years, however, to analytically establish the existence of soliton solutions to the FPUT problem [54].

Toda lattice The Toda lattice [125, 126] is a classical example of a fully integrable discrete system that also admits solitary waves as solution. It can be written as

$$\ddot{u}_j = e^{-(u_j - u_{j-1})} - e^{-(u_{j+1} - u_j)}. \tag{1.1.6}$$

Here $u_j(t)$ represents the horizontal displacement of the jth element at time t. The Toda lattice system has been used to model certain mechanics of DNA strands at body temperature [97, 98].

It was shown by Chen and Liu [26] that a discrete Bäcklund Transform can be used to construct more complex solutions to (1.1.6) by combining multiple solitary waves. The stability of such $n-$soliton solutions was proved only recently by Benes, Hoffman and Wayne [11] through the use of so-called Bäcklund Transform ladders, where the Bäcklund Transform is applied iteratively to reduce the complexity of the problem.

FitzHugh-Nagumo The FitzHugh-Nagumo model is a two component system devised by FitzHugh [52] and Nagumo [99] in order to recreate the dynamics of signal transmissions along the axon of a neuron. The axon is a nerve fiber which is covered by a myelin coating. However, this coating admits gaps at regular distances (about every 1mm) along the fiber. These gaps are about 1μm in length and are called Nodes of Ranvier.

The model tries to encompass the most essential characteristics of a ion flow in a sodium-potassium media via two equations. The first one is related to the voltage, while the second one describes a recovery variable. The strength of this approach is that it is able to capture the recessive phase that appears right after the passage of a strong enough signal.

The standard formulation in continuous spatial coordinates is

$$\begin{cases} \dot{v} &= v_{xx} + g(v,a) - w, \\ \dot{w} &= \rho(v - \gamma w), \end{cases} \tag{1.1.7}$$

in which $g(v,a) = v(1-v)(v-a)$ is a bistable cubic nonlinearity and ρ and γ are positive parameters. A great deal of attention has been spent on this system: the singular limit $\rho \downarrow 0$ regime has for example strongly influenced the development of geometric singular perturbation theory; see [24, 63, 78, 79, 80, 86].

It turns out to be advantageous to consider how signals jump from one Node of Ranvier to the next, while ignoring the dynamics through the myelin coating between the two nodes [9, 72]. In particular, let us switch to a spatially discrete setting by replacing $v(x,t)$ and $w(x,t)$ with $v_j(t)$ and $w_j(t)$ respectively. In addition we replace the diffusion v_{xx} by its nearest neighbour counterpart $v_{j-1} - 2v_j + v_{j+1}$, thus obtaining

$$\begin{cases} \dot{v}_j &= (v_{j-1} - 2v_j + v_{j+1}) + g(v_j,a) - w_j, \\ \dot{w}_j &= \rho(v_j - \gamma w_j). \end{cases} \tag{1.1.8}$$

In recent years there have been substantial developments regarding the existence [72, 48, 114] and stability [73, 113] of travelling pulses for (1.1.8) and some of its extensions.

Nagumo In 1960 John W. Cahn devised a model to describe the growth of crystals on atomic scales [20]. The main feature of this model is that the boundary of the crystaline formation can be represented by a front that moves slowly through the domain. The PDE that he considered is

$$u_t = u_{xx} + g(u, a), \tag{1.1.9}$$

with $g(u, a) = u(1 - u)(u - a)$.

A few years later Mitio Nagumo [94] independently used the same equation to describe similar dynamics among populations invading spatial domains. For this reason equation (1.1.9) is known both as the Allen-Cahn [2] and the Nagumo equation. It is well known [50] that equation (1.1.9) admits a solution in the form of a travelling front $u(x, t) = \varphi(x - ct)$, for some $c \in \mathbb{R}$ and wave profile φ that satisfies

$$\lim_{\xi\to-\infty} \varphi(\xi) = 0, \quad \lim_{\xi\to\infty} \varphi(\xi) = 1. \tag{1.1.10}$$

If we plug this Ansatz into (1.1.9) we obtain

$$-c\varphi'(\xi) = \varphi''(\xi) + g(\varphi(\xi), a), \tag{1.1.11}$$

a fairly standard second order ODE.

The natural way to transfer this model to a spatially discrete setting is to write

$$\dot{u}_j = d(u_{j-1} - 2u_j + u_{j+1}) + g(u_j, a), \tag{1.1.12}$$

with $j \in \mathbb{Z}$. Here the diffusion coefficient d is directly related to the discretization distance h. Indeed, using the approximation $u_{xx}(x) = (u(x - h) - 2u(x) + u(x + h))/h^2 + O(h^3)$ and assuming $u_j = u(jh)$, we see that is natural to take $d \sim h^{-2}$ to bring us from the continuous to the discrete formulation.

If we now look for a travelling front of the form $u_j(t) = \varphi(j - ct)$, we find that such a solution must satisfy

$$-c\varphi'(\xi) = d(\varphi(\xi - 1) - 2\varphi(\xi) + \varphi(\xi + 1)) + g(\varphi(\xi), a). \tag{1.1.13}$$

In the PDE setting it is easy to show that the speed coefficient c of the travelling solution is negative when $a < \frac{1}{2}$ and positive if $a > \frac{1}{2}$. This also implies that the wavespeed vanishes[1] whenever $a = \frac{1}{2}$. When we move to the LDE setting however, one encounters a new phenomenon, called *propagation failure*. More specifically, there exists a small buffer interval $[\frac{1}{2} - \varepsilon, \frac{1}{2} + \varepsilon]$ for a inside of which we have pinned solutions (i.e. $c = 0$). This phenomenon has been studied extensively, both analytically [21, 67,

[1] due to the point symmetry that $g(u, \frac{1}{2}) = u(\frac{1}{2} - u)(1 - u)$ possesses with respect to $u = \frac{1}{2}$.

70, 83, 92, 40] and numerically [1, 42, 44, 55]. Propagation failure is guaranteed to occur when the diffusion coefficient d is sufficiently small, but in general it is highly dependent on the shape of the nonlinearity g. In Chapter 2 we will see some numerical simulations for the null speed threshold in the parameter region $(a, d) \in [0, 1] \times \mathbb{R}^+$.

Throughout this thesis we will analyze the Lattice Nagumo equation (1.1.12) together with its planar counterpart. In particular, we show that it is possible to obtain a range of solutions that can be seen as variations of the classical travelling waves.

1.2 Multichromatic travelling waves

Many examples in nature, ranging from polymer dynamics [122] to DNA strings [35, 135], feature spatial structures that are not constant but rather periodically distributed. This tells us that besides considering globally constant steady states and parameters, it might be worthwhile to investigate systems that exhibit periodic behaviour or possess periodic parameters.

While [46] and [114] analyze LDEs with periodic parameters, in this thesis we will investigate periodic steady states. More in detail, we will consider the Nagumo problem on regular lattices and look for waves that have $n-$periodical asymptotic values.

1.2.1 Bichromatic waves

As a first step, let us separate the equations for the even and odd nodes in the lattice. This can be achieved by looking for solutions to (1.1.12) of the form

$$u_j(t) = \begin{cases} \Phi_e(j - ct) & \text{if } j \text{ is even,} \\ \Phi_o(j - ct) & \text{if } j \text{ is odd,} \end{cases} \tag{1.2.1}$$

for some speed c and profile waves $(\Phi_o, \Phi_e) : \mathbb{R} \to \mathbb{R}^2$. If we plug this Ansatz into (1.1.12) we obtain

$$\begin{cases} -c\Phi_o'(\xi) = d(\Phi_e(\xi - 1) + \Phi_e(\xi + 1) - 2\Phi_o(\xi)) + g(\Phi_o(\xi), a), \\ -c\Phi_e'(\xi) = d(\Phi_o(\xi - 1) + \Phi_o(\xi + 1) - 2\Phi_e(\xi)) + g(\Phi_e(\xi), a). \end{cases} \tag{1.2.2}$$

Rather than considering asymptotic conditions such as (1.1.10), we can now impose the two-periodic limit values

$$\lim_{\xi \to -\infty} (\Phi_o(\xi), \Phi_e(\xi)) = (0, 0), \quad \lim_{\xi \to \infty} (\Phi_o(\xi), \Phi_e(\xi)) = (\overline{u}_o, \overline{u}_e), \tag{1.2.3}$$

for some $\overline{u}_o, \overline{u}_e \in (0, 1)$. The couple $(\overline{u}_o, \overline{u}_e)$ in (1.2.3) cannot be chosen arbitrarily, but it must satisfy the stationary conditions

$$\begin{cases} 0 = 2d(\overline{u}_e - \overline{u}_o) + g(\overline{u}_o, a), \\ 0 = 2d(\overline{u}_o - \overline{u}_e) + g(\overline{u}_e, a). \end{cases} \tag{1.2.4}$$

From (1.2.4) we see that $\overline{u}_o$ and $\overline{u}_e$ must satisfy

$$g(\overline{u}_o, a) + g(\overline{u}_e, a) = 0, \tag{1.2.5}$$

independently from the value of d. Assuming $a \leq 1/2$, we can define for $u \in (0, a)$ the functions

$$\begin{aligned} u_e^-(u;a) &= \min\{g^{-1}(-g(u,a),a)\}, \\ u_e^+(u;a) &= \max\{g^{-1}(-g(u,a),a)\}. \end{aligned} \tag{1.2.6}$$

If $u \in \{0, a\}$, then we can use continuity to define

$$u_e^-(0;a) = u_e^-(a;a) = a, \qquad u_e^+(0;a) = u_e^+(a;a) = 1. \tag{1.2.7}$$

Geometrically, for any given $u \in [0, a]$ these functions represent the two solutions that (1.2.5) possesses.

Inspired by the first equation of (1.2.4), let us furthermore define the function

$$u_e^d(u;d,a) := u - g(u,a)/2d. \tag{1.2.8}$$

All that is needed for a couple $(\overline{u}_o, \overline{u}_e)$ to be a solution of (1.2.4) is that $u_e^{\pm}(\overline{u}_o;a) = u_e^d(\overline{u}_o;d,a) = \overline{u}_e$, see the left graph in Figure 1.1. Motivated by this, let us introduce the set of couples $(a,d) \in [0,1] \times \mathbb{R}^+$ for which we have two distinct solutions to $u_e^+(\overline{u}_o) = u_e^d(\overline{u}_o;d,a)$ with $\overline{u}_o \in (0,1)$, and let us call this set Ω_{bc}, see the right graph in Figure 1.1.

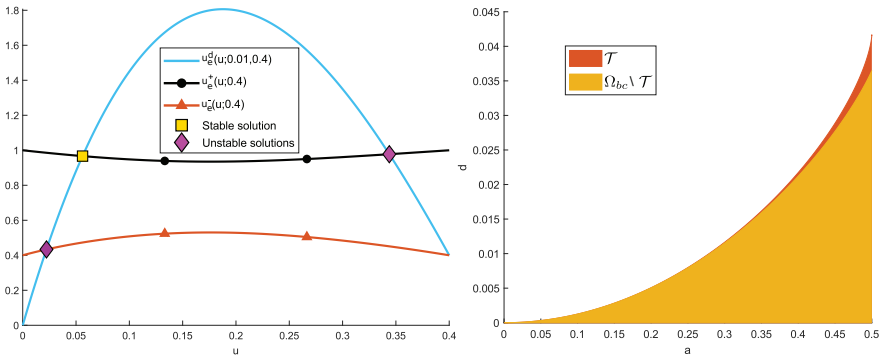

Figure 1.1: On the left, the graphs of u_e^d and $u_e^{\pm}$ for $(a,d) = (0.4, 0.01) \in \Omega_{bc}$. On the right, the region Ω_{bc} and its subregion $\mathcal{T}$ where we find a nonzero speed for the front connecting the heterogeneous stable steady state to the homogeneous state $(1,1)$. For $a \in [0.5, 1]$ these regions can be reflected through the line $a = \frac{1}{2}$.

Travelling fronts The general theory in [27] allows us to find wave solutions connecting the stable heterogeneous steady states with the homogeneous ones $(0,0)$ and $(1,1)$. A natural question is, thus, whether such solutions actually travel or stand still. Inside of Ω_{bc} we can find a region $\mathcal{T}$, see the right graph in Figure 1.1, where the wave profile connecting the stable heterogeneous root to the homogeneous state $(1,1)$ has a nonzero speed.

In Chapter 2 we will analyze this region in depth. We will manage to find analytic expansions for Ω_{bc}'s upper boundary around $a = 0$ (and by symmetry $a = 1$) and around its cusp in $(a,d) = (\frac{1}{2}, \frac{1}{24})$. We also derive a geometric condition to conclude $(a,d) \in \mathcal{T}$, which guarantees that $\mathcal{T}$ is not empty. In Chapter 3 we will investigate trichromatic and quadrichromatic dynamics and we will show that even richer results can be obtained.

1.2.2 Custom nonlinearity

Although in this thesis we will only consider the polynomial nonlinearities $g(u,a) = u(1-u)(u-a)$ or $g(u,a) = (1-u^2)(u-a)$, it is interesting to think about what happens with "slightly" different bistable functions.

In Section 2.3 we will see that some computations heavily rely on the geometry of the cubic. Even though such an approach does not appear to be as general as one would hope for, a quick way to recognize its value is to consider a different custom-made bistable nonlinearity, namely

$$g_{cus}(u,a) = \begin{cases} \dfrac{2(u-a)u(81a^2 - 208au + 176u^2)}{a^3} & u \le a, \\ \dfrac{(1-u)(u-a)}{20(a-1)^4}[5292u^3 + u^2(-10116a - 5760) & \\ +u(3993a^2 + 12246a - 363) - 1129a^3 - 606a^2 - 5517a + 1960] & u > a. \end{cases} \tag{1.2.9}$$

In accordance with the third order polynomial g, we see that g_{cus} has only one local minimum in $[0,a]$ and one local maximum in $[a,1]$. Moreover, we have $g_{cus}(\cdot,a) \in C^1([0,1])$, $\forall a \in [0,1]$. In Figure 1.2 we can see the graph of $g_{cus}(\cdot, 0.4)$ together with a multiple of the standard cubic $g(u,a) = u(1-u)(u-a)$.

Due to the shape that g_{cus} has in $[0,a]$, we can observe from Figure 1.3 that the function $u_e^d(u;d,a)$ can have two local maximum points. In particular, we can define a region $\Omega_{bc}^{(1)}$ where u_e^d and u_e^+ have two intersection points, together with a region $\Omega_{bc}^{(2)}$ where $u_e^+(u;a)$ and $u_e^d(u;d,a)$ cross in four different points.

Travelling fronts It is possible to numerically check if there exist moving connections between the various steady states. As before, in $\Omega_{bc}^{(1)}$ there is a region $\mathcal{T}$ where the heterogeneous stable steady state is connected to 1 via a moving front. In $\Omega_{bc}^{(2)}$, however, we do not find any wave solution that possesses a nonzero speed and

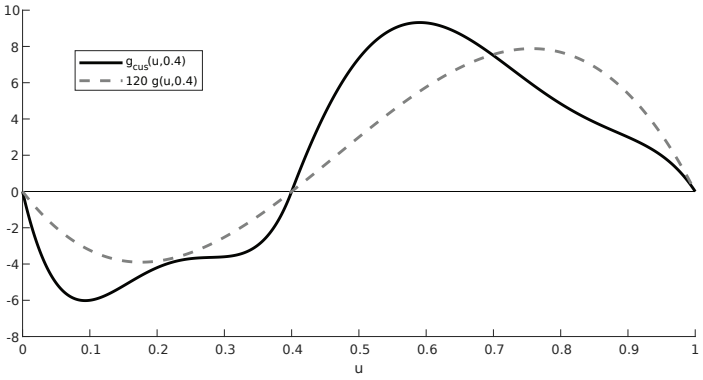

Figure 1.2: Graph of $g_{cus}(\cdot, 0.4)$ compared to a multiple of the standard cubic $g(\cdot, 0.4)$. Through (1.2.4) and (1.2.8) we see how a multiplication of the nonlinearity g or g_{cus} can be dealt with by rescaling d in the same way.

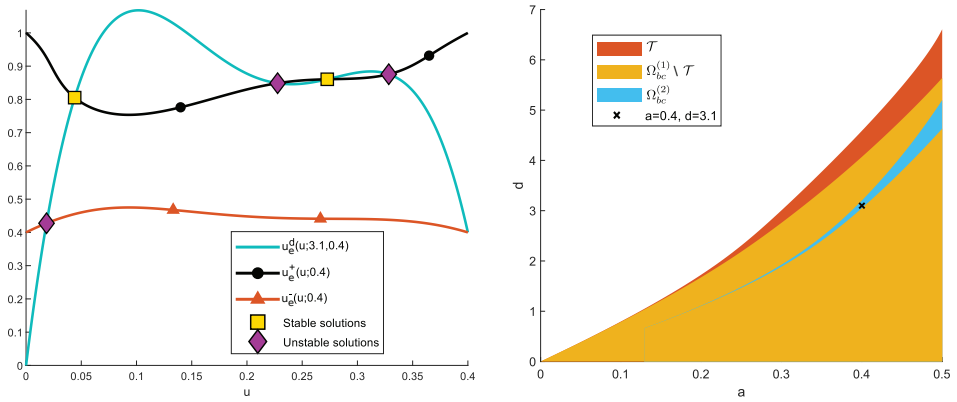

Figure 1.3: On the left, we can see the intersections between u_e^d with u_e^+ and u_e^- for $a = 0.4$ and $d = 3.1$ for g_{cus}. On the right, the numerically computed regions $\Omega_{bc}^{(1)}$ and $\Omega_{bc}^{(2)}$, together with the $\mathcal{T}$ region.

connects any two of the four stable steady states (namely 0, 1 and the two stable heterogeneous solutions depicted in Figure 1.3).

1.3 Planar systems

Let us now explore systems with two spatial dimensions. What might first come to mind when thinking about dynamics evolving on bidimensional surfaces, especially if you happen to live in the Netherlands, is probably the weather forecast [107, 88]. There is, however, an incredible richness of other phenomena that can be efficiently studied with planar models, for example in biology [127, 116, 39], chemistry [133] or signal processing [33].

When increasing the number of spatial dimensions, we usually find two types of theoretical challenges. The first one is how to transfer results from lower dimensional frames into the higher dimensional setting, which often brings new technical obstacles. In the next pages we will shortly introduce some possible planar extensions to mono- and multichromatic dynamics. Even though we only analyze unidimensional lattices in Chapters 2 and 3, we will see in the following pages that most of the theory can be directly exported to bidimensional lattice dynamics.

The second challenge revolves around the identification of new phenomena that can arise. In Chapter 4 we will discuss a class of bidimensional travelling patterns that does not possess any lower dimensional counterpart.

1.3.1 Bidimensional Nagumo PDE

Let us consider the extension of the standard Nagumo PDE (1.1.9) onto the two-dimensional plane $\mathbb{R}^2$. We now have to take care of the diffusion operator and make sure that it encompasses both spatial directions, so let us write

$$u_t = (\partial_{xx} + \partial_{yy})u + g(u, a). \tag{1.3.1}$$

Looking for a solution that travels along a direction $\theta \in [0, 2\pi]$, we write

$$u(x, y, t) = \varphi(\cos(\theta)x + \sin(\theta)y - ct). \tag{1.3.2}$$

The equation that needs to be solved by φ is now

$$-c\varphi'(\xi) = (\cos^2(\theta) + \sin^2(\theta))\varphi''(\xi) + g(\varphi(\xi), a) = \varphi''(\xi) + g(\varphi(\xi), a), \tag{1.3.3}$$

which coincides perfectly with (1.1.11). Note that this ODE does not depend on the angle θ, due to the radial symmetry that $\mathbb{R}^2$ possesses.

Nevertheless, the planar setting does pose some challenges. We must remark now that a front travelling on $\mathbb{R}$ only possesses a bounded area where it takes values u with $0 < \varepsilon < u < 1 - \varepsilon < 1$, for any $\varepsilon > 0$. In higher dimensions however we usually find an infinite region where the solution takes such values. One must therefore take care when choosing an appropriate class of admissible perturbations.

Nevertheless in [82] Kapitula manages to prove the asymptotic stability of multi-dimensional travelling fronts. In addition, in [13] the authors establish the asymptotic stability of bidimensional fronts when encountering bounded obstacles, while in [4] localized initial profiles are shown to be able to expand through the whole spatial domain.

1.3.2 Square lattices

The most natural way to formulate the Nagumo equation on $\mathbb{Z}^2$ is to include the four nearest neighbours into the action of the diffusion operator, so that (1.1.12) becomes

$$\dot{u}_{i,j}(t) = d\left(u_{i,j-1}(t) + u_{i,j+1}(t) + u_{i-1,j}(t) + u_{i+1,j}(t) - 4u_{i,j}(t)\right) + g(u_{i,j}(t), a). \tag{1.3.4}$$

Let us consider again travelling solutions moving along the direction θ, by writing

$$u_{i,j}(t) = \varphi(\cos(\theta)i + \sin(\theta)j - ct). \tag{1.3.5}$$

In order to solve (1.3.4), we see that the pair (c, Φ) needs to satisfy

$$-c\varphi'(\xi) = d(\varphi(\xi+\cos(\theta))+\varphi(\xi-\cos(\theta))+\varphi(\xi+\sin(\theta))+\varphi(\xi-\sin(\theta))-4\varphi(\xi))+g(\varphi(\xi), a), \tag{1.3.6}$$

where we can clearly see a dependency on the angle θ. Solutions of this type were constructed in [91].

As in the unidimensional case, the propagation failure phenomenon plays an important role in the study of (1.3.4). Due to the presence of the new angular parameter θ, the speed now depends greatly on the direction the travelling front is facing. This dependence can be rather intricate, up to the point of waves being pinned in certain directions but travelling in others [21, 66, 67].

1.3.2.1 Bichromatic Nagumo LDE on square lattices

Let us consider the bidimensional system (1.3.4), and let us assume that for some angle $\theta \in [0, 2\pi)$ there exists a travelling solution of the form

$$u_{i,j}(t;\theta) = \begin{cases} \Phi_e(\cos(\theta)i + \sin(\theta)j - ct) & \text{if } i+j \text{ is even,} \\ \Phi_o(\cos(\theta)i + \sin(\theta)j - ct) & \text{if } i+j \text{ is odd.} \end{cases} \tag{1.3.7}$$

If we plug the Ansatz (1.3.7) into (1.3.4), we obtain

$$\begin{cases} -c\Phi_e'(\xi) = & d(\Phi_o(\xi+\cos(\theta)) + \Phi_o(\xi-\cos(\theta)) + \Phi_o(\xi+\sin(\theta)) + \Phi_o(\xi-\sin(\theta)) \\ & -4\Phi_e(\xi)) + g(\Phi_e(\xi), a), \\ -c\Phi_o'(\xi) = & d(\Phi_e(\xi+\cos(\theta)) + \Phi_e(\xi-\cos(\theta)) + \Phi_e(\xi+\sin(\theta)) + \Phi_e(\xi-\sin(\theta)) \\ & -4\Phi_o(\xi)) + g(\Phi_o(\xi), a), \end{cases} \tag{1.3.8}$$

which closely resembles the MFDE (1.1.13). In the same fashion as in the unidimensional case we see that a steady state couple $(\overline{u}_e, \overline{u}_o)$ would have to satisfy

$$\begin{cases} 0 = 4d(\overline{u}_o - \overline{u}_e) + g(\overline{u}_e, a), \\ 0 = 4d(\overline{u}_e - \overline{u}_o) + g(\overline{v}_o, a), \end{cases} \tag{1.3.9}$$

the solutions of which can be obtained by the ones for (1.2.4) by simply rescaling the diffusion parameter to $\widetilde{d} = 2d$.

We can find some additional similarities with the unidimensional dynamic. If we set $\theta = \pi/4 + k\pi/2$, the system (1.3.8) takes the form

$$\begin{cases} -c\Phi_e'(\xi) = 2d(\Phi_o(\xi + \sqrt{2}/2) + \Phi_o(\xi - \sqrt{2}/2) - 2\Phi_e(\xi)) + g(\Phi_e(\xi), a), \\ -c\Phi_o'(\xi) = 2d(\Phi_e(\xi + \sqrt{2}/2) + \Phi_e(\xi - \sqrt{2}/2) - 2\Phi_o(\xi)) + g(\Phi_o(\xi), a), \end{cases} \tag{1.3.10}$$

which can be seen as the unidimensional bichromatic travelling wave problem (1.2.2) on $\frac{\sqrt{2}}{2}\mathbb{Z}$ with a new diffusion parameter $\widetilde{d} = 2d$. In Section 4.2 we will numerically examine the full dependence of c on θ.

1.3.3 Hexagonal lattices

Another common type of regular planar lattice that is encountered in real-world applications is the unitary hexagonal lattice. Since the theoretical discovery of graphene [133] as a single layer of a graphite structure in 1947, and especially since its actual isolation [101] in 2004, the hexagonal lattice has risen in popularity.

In order to best approach the study of planar travelling waves on such lattices it is convenient to make a distinction between *top* and *bottom* vertices (as seen from the perspective of the embedded hexagons). In Figure 1.4 we can see how the *top* vertices are coloured in green and the *bottom* ones are coloured in red.

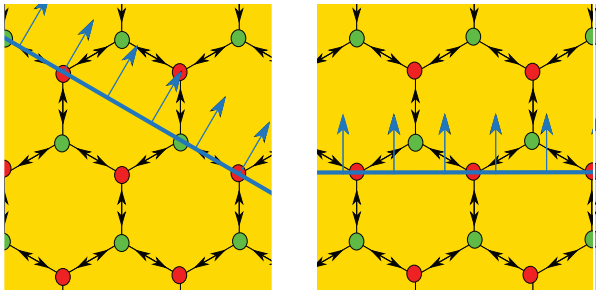

Figure 1.4: Two examples of travelling fronts that are aligned with the hexagonal structure, with $\theta = \pi/3$ on the left and $\theta = \pi/2$ on the right. Here we used red dots to represent the *bottom* edges and green dots for the *top* ones.

Since we will be dealing with planar waves, the most natural way to address the vertices is by their cartesian coordinates. We can choose an arbitrary *bottom* edge as the origin. Given the asymmetry between *top* and *bottom* vertices, let us split our system in two separate components:

$$\begin{cases} \dot{u}_t = d\Delta^{\curlywedge}(u_b, u_t) + g(u_t, a), \\ \dot{u}_b = d\Delta^{\curlyvee}(u_t, u_b) + g(u_b, a). \end{cases} \tag{1.3.11}$$

Here the top- and bottom-diffusion operators $\Delta^{\curlywedge}$ respectively $\Delta^{\curlyvee}$ are defined as

$$\begin{aligned}\Delta^{\curlywedge}(u_b,u_t)(x,y) &= u_b(x,y+1)+u_b\left(x-\frac{\sqrt{3}}{2},y-\frac{1}{2}\right)+u_b\left(x+\frac{\sqrt{3}}{2},y-\frac{1}{2}\right)-3u_t(x,y),\\ \Delta^{\curlyvee}(u_t,u_b)(x,y) &= u_t\left(x+\frac{\sqrt{3}}{2},y+\frac{1}{2}\right)+u_t\left(x-\frac{\sqrt{3}}{2},y+\frac{1}{2}\right)+u_t(x,y-1)-3u_b(x,y).\end{aligned} \tag{1.3.12}$$

Let us remark that every *top* edge is connected uniquely with three *bottom* edges and conversely, every *bottom* edge is connected uniquely to three *top* edges.

Let us assume that for some $\theta, c \in \mathbb{R}$, we have found a travelling solution

$$(u_t,u_b)(x,y,t) = (\phi_t,\phi_b)(\cos(\theta)x+\sin(\theta)y-ct) \tag{1.3.13}$$

that satisfies (1.3.11). By plugging (ϕ_t,ϕ_b) into (1.3.11), we obtain the new system

$$\begin{cases} -c\phi_t'(\xi) = d(\phi_b(\xi+r_1)+\phi_b(\xi+r_2)+\phi_b(\xi+r_3)-3\phi_t(\xi))+g(\phi_t,a),\\ -c\phi_b'(\xi) = d(\phi_t(\xi+r_4)+\phi_t(\xi+r_5)+\phi_t(\xi+r_6)-3\phi_b(\xi))+g(\phi_b,a),\end{cases} \tag{1.3.14}$$

with

$$\begin{aligned} r_1 &= \cos(\pi/2-\theta), & r_4 &= \cos(\pi/6-\theta),\\ r_2 &= \cos(7\pi/6-\theta), & r_5 &= \cos(5\pi/6-\theta),\\ r_3 &= \cos(11\pi/6-\theta), & r_6 &= \cos(3\pi/2-\theta).\end{aligned} \tag{1.3.15}$$

Due to the bichromatic splitting we had to enforce, it seems natural to consider asymptotic conditions such as

$$\begin{aligned}\lim_{\xi\to-\infty}(\phi_t,\phi_b)(\xi) &= (0,0),\\ \lim_{\xi\to\infty}(\phi_t,\phi_b)(\xi) &= (\overline{u}_t,\overline{u}_b).\end{aligned} \tag{1.3.16}$$

By inspecting the system (1.3.11), we see that $\overline{u}_t$ and $\overline{u}_b$ this time must satisfy the steady state conditions

$$\begin{cases} 0 = 3d(\overline{u}_b-\overline{u}_t)+g(\overline{u}_t,a),\\ 0 = 3d(\overline{u}_t-\overline{u}_b)+g(\overline{u}_b,a).\end{cases} \tag{1.3.17}$$

We can hence again borrow existence results for the heterogeneous solutions from the unidimensional setting after rewriting $\widetilde{d} = \frac{3}{2}d$.

It is furthermore possible to choose $\overline{u}_t = \overline{u}_b = 1$ and obtain a front (still composed of two different functions ϕ_t and ϕ_b) that connects the two stable homogeneous states.

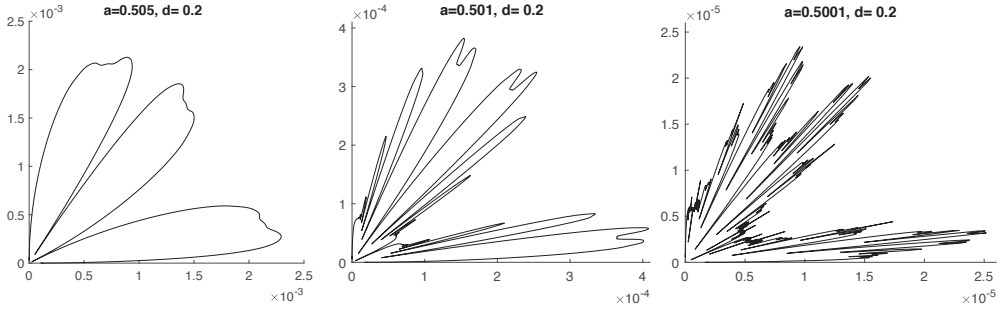

Figure 1.5: Radial speed for the travelling wave connecting $(0,0)$ to $(1,1)$ on the regular hexagonal lattice for different values of a. These curves correspond to $(\cos(\theta)c(\theta), \sin(\theta)c(\theta))$.

Travelling fronts Similarly as for the square lattice, we can numerically compute the speed of the bichromatic fronts on hexagonal lattices. In Figure 1.5 we see how the speed of the fronts connecting $(0,0)$ and $(1,1)$ varies when changing the direction θ, for three values of a close to the critical case $a = \frac{1}{2}$.

On the other hand, in Figure 1.6 we can observe how the radial speed changes when reducing the diffusion parameter d for the travelling front connecting $(0,0)$ to the stable heterogeneous rest state $(\overline{u}_t, \overline{u}_b)$. Let us remark that these plots are computed for $a = 0.5$, where we cannot find travelling fronts connecting the homogeneous states. Even though the speed values are fairly uniform for higher diffusion coefficients, we see that when d decreases the main lattice directions $\theta = k\pi/6$ are subject to more variations than the other non-aligned directions.

1.3.3.1 Multichromatic fronts on hexagonal lattices

It is no longer a straightforward exercise to come up with periodic colouring schemes for which a corresponding wave equation can be formulated. We will now shortly introduce the two most immediate examples.

The first one uses a 6-colours pattern as illustrated in Figure 1.7. The values B, D and F always appear on the *top* vertices while A, C and E correspond with the

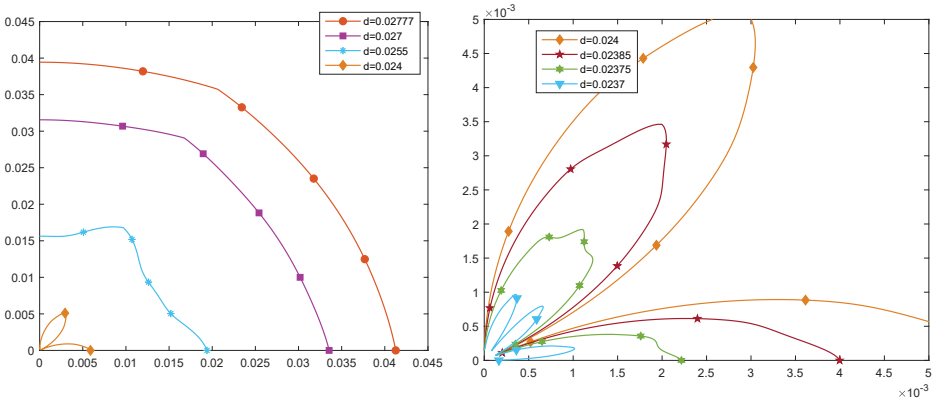

Figure 1.6: Radial speed for the bichromatic wave posed on the regular hexagonal lattice for $a = 0.5$. Notice the quicker speed reduction along the directions corresponding to the lattice orientation.

bottom ones. The wave equation associated to this system is

$$\begin{cases} -cA'(\xi) = d(B(\xi+r_4) + D(\xi+r_5) + F(\xi+r_6) - 3A(\xi)) + g(A(\xi), a), \\ -cB'(\xi) = d(E(\xi+r_1) + A(\xi+r_2) + C(\xi+r_3) - 3B(\xi)) + g(B(\xi), a), \\ -cC'(\xi) = d(F(\xi+r_4) + B(\xi+r_5) + D(\xi+r_6) - 3C(\xi)) + g(C(\xi), a), \\ -cD'(\xi) = d(C(\xi+r_1) + E(\xi+r_2) + A(\xi+r_3) - 3D(\xi)) + g(D(\xi), a), \\ -cE'(\xi) = d(D(\xi+r_4) + F(\xi+r_5) + B(\xi+r_6) - 3E(\xi)) + g(E(\xi), a), \\ -cF'(\xi) = d(A(\xi+r_1) + C(\xi+r_2) + E(\xi+r_3) - 3F(\xi)) + g(F(\xi), a). \end{cases} \tag{1.3.18}$$

It is easy to see that any 6-valued heterogeneous rest state $(\overline{A}, \overline{B}, \overline{C}, \overline{D}, \overline{E}, \overline{F}) \in [0,1]^6$ must satisfy the system

$$\begin{cases} 0 = d(\overline{B} + \overline{D} + \overline{F} - 3\overline{A}) + g(\overline{A}, a), \\ 0 = d(\overline{A} + \overline{C} + \overline{E} - 3\overline{B}) + g(\overline{B}, a), \\ 0 = d(\overline{B} + \overline{D} + \overline{F} - 3\overline{C}) + g(\overline{C}, a), \\ 0 = d(\overline{A} + \overline{C} + \overline{E} - 3\overline{D}) + g(\overline{D}, a), \\ 0 = d(\overline{B} + \overline{D} + \overline{F} - 3\overline{E}) + g(\overline{E}, a), \\ 0 = d(\overline{A} + \overline{C} + \overline{E} - 3\overline{F}) + g(\overline{F}, a). \end{cases} \tag{1.3.19}$$

It is interesting to note that this algebraic system also arises when considering the equilibria of the Nagumo equation

$$\dot{u}_v = d \sum_{w \sim v} (u_w - u_v) + g(u_v, a) \tag{1.3.20}$$

posed on the graph $v \in K_{3,3}$ depicted on the left of Figure 1.9. Here the relation $w \sim v$ means that the vertices v and w are connected. In particular, the one dimensional theory developed in Chapters 2 and 3 can no longer be applied to this situation. However, the algebraic system (1.3.19) can be simplified by taking $\overline{B} = \overline{D} = \overline{F} = \overline{u}_t$ and $\overline{A} = \overline{C} = \overline{E} = \overline{u}_b$, in which case (1.3.19) and (1.3.18) get simplified to (1.3.17) and (1.3.14) respectively.

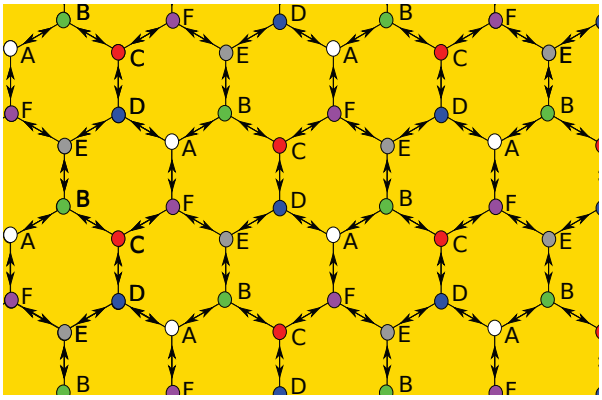

Figure 1.7: The 6-colour pattern corresponding with (1.3.18) and (1.3.19).

The final multichromatic pattern that we are going to consider on the hexagonal lattice is the 8-coloured one depicted in Figure 1.8. The corresponding wave system

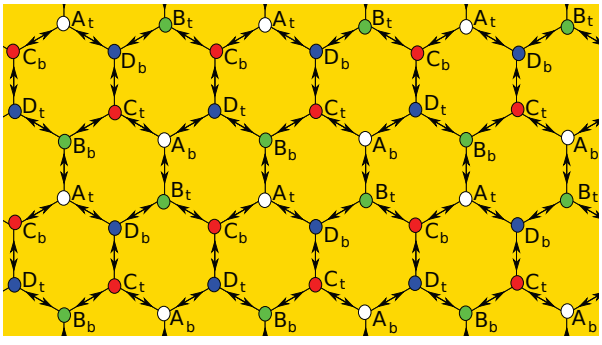

Figure 1.8: The 8-colour pattern corresponding with (1.3.21) and (1.3.23).

for the eight variables is

$$\begin{cases} -cA_t'(\xi) = d(B_b(\xi+r_1) + C_b(\xi+r_2) + D_b(\xi+r_3) - 3A_t(\xi)) + g(A_t(\xi), a), \\ -cA_b'(\xi) = d(D_t(\xi+r_4) + C_t(\xi+r_5) + B_t(\xi+r_6) - 3A_b(\xi)) + g(A_b(\xi), a), \\ -cB_t'(\xi) = d(A_b(\xi+r_1) + D_b(\xi+r_2) + C_b(\xi+r_3) - 3B_t(\xi)) + g(B_t(\xi), a), \\ -cB_b'(\xi) = d(C_t(\xi+r_4) + D_t(\xi+r_5) + A_t(\xi+r_6) - 3B_b(\xi)) + g(B_b(\xi), a), \\ -cC_t'(\xi) = d(D_b(\xi+r_1) + B_b(\xi+r_2) + A_b(\xi+r_3) - 3C_t(\xi)) + g(C_t(\xi), a), \\ -cC_b'(\xi) = d(A_t(\xi+r_4) + B_t(\xi+r_5) + D_t(\xi+r_6) - 3C_b(\xi)) + g(C_b(\xi), a), \\ -cD_t'(\xi) = d(C_b(\xi+r_1) + A_b(\xi+r_2) + B_b(\xi+r_3) - 3D_t(\xi)) + g(D_t(\xi), a), \\ -cD_b'(\xi) = d(B_t(\xi+r_4) + A_t(\xi+r_5) + C_t(\xi+r_6) - 3D_b(\xi)) + g(D_b(\xi), a). \end{cases} \tag{1.3.21}$$

We can in general consider eight different asymptotic values for the variables $(A_t, A_b, B_t, B_b, C_t, C_b, D_t, D_b)$. The corresponding steady-state system is then equivalent to that of the Nagumo equation on the cubic graph, see Figure 1.9.

As the naming and colouring suggests, however, we are interested in the case where we only have to provide the four asymptotic values

$$\begin{aligned} \lim_{\xi\to\infty} A_t(\xi) = \lim_{\xi\to\infty} A_b(\xi) = \overline{A}, \\ \lim_{\xi\to\infty} B_t(\xi) = \lim_{\xi\to\infty} B_b(\xi) = \overline{B}, \\ \lim_{\xi\to\infty} C_t(\xi) = \lim_{\xi\to\infty} C_b(\xi) = \overline{C}, \\ \lim_{\xi\to\infty} D_t(\xi) = \lim_{\xi\to\infty} D_b(\xi) = \overline{D}. \end{aligned} \tag{1.3.22}$$

In order to find the heterogeneous steady state quadruplets $(\overline{A}, \overline{B}, \overline{C}, \overline{D})$ we would then need to solve

$$\begin{cases} 0 = d(\overline{B} + \overline{C} + \overline{D} - 3\overline{A}) + g(\overline{A}, a), \\ 0 = d(\overline{A} + \overline{C} + \overline{D} - 3\overline{B}) + g(\overline{B}, a), \\ 0 = d(\overline{A} + \overline{B} + \overline{D} - 3\overline{C}) + g(\overline{C}, a), \\ 0 = d(\overline{A} + \overline{B} + \overline{C} - 3\overline{D}) + g(\overline{D}, a), \end{cases} \tag{1.3.23}$$

which can only be further reduced by taking $\overline{A} = \overline{B} = \overline{C} = \overline{D}$.

The interesting feature of the steady state system (1.3.23) is that it corresponds to the complete graph K_4; see Figure 1.9. Following the steps of [121], we will see in Chapter 3 that the steady state equation for the unidimensional trichromatic waves can be related to the Nagumo system on K_3, while K_2 is associated to the bichromatic problem[2] discussed in Chapter 2 and Section 1.2.1 above.

For completeness let us mention that the periodic extension of the Nagumo system on K_5 must be posed on $\mathbb{Z}^2$. On the other hand, K_6 does not admit a regular planar

[2] With a proper readjustment of the diffusion parameter d.

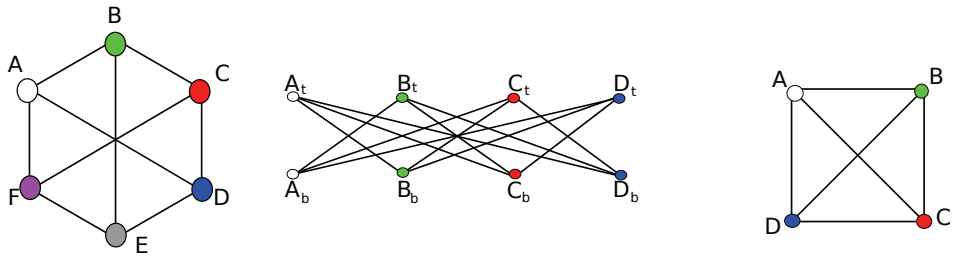

Figure 1.9: On the left, the bipartite graph $K_{3,3}$ that generates (1.3.19), also known as the utility graph. In the centre, the crown S_4^0 graph that generates the 8-coloured steady states system for $(A_t, A_b, B_t, B_b, C_t, C_b, D_t, D_b)$, also known as the cubic graph. On the right, the complete graph K_4 that generates the reduced system (1.3.23).

extension, but K_7 can be recovered from a triangular planar lattice (or $\mathbb{Z}^3$). The graph K_5 does not seem to admit any novel behaviour, but the wave equation for K_7 turned out to be computationally too cumbersome for a detailed analysis.

1.3.4 Beyond waves: travelling corners

Upon looking at the system (1.3.4), one might wonder about the behaviour of travelling profiles whose initial shape is close to a perfectly planar front except for some type of defect. The subject is a good starting point if we are interested in studying the microscopic dynamics of crystal growth, which is closely related to Wulff shapes [108, 136].

The results in [61] show that only interior corners can be found for the standard Nagumo PDE, while in [60] a whole range of defects (interior corners, exterior corners, steps or holes) can arise if a (small) amount of spatial heterogeneity is added to the system.

In Chapter 4 we will establish the existence of interior and exterior corners in the bidimensional LDE setting, with the presence of one excluding the other. We will also briefly investigate such defects in the context of bidimensional bichromatic travelling waves. This study is a perfect example of how it is possible to construct more complex moving structures starting from simple travelling waves.